Model-based controller design for a lift-and-drop railway track switch actuator

Precious Lorraine Kaijuka*, Roger Dixon, Christopher Patrick Ward, Saikatt Dutta and Samuel Bemment

***Abstract*—Track switches are essential in order to enable railway vehicles to change routes however they are also the largest single cause of failure on the railway network. A new generation of switching concepts are emerging from projects like In2Rail, REPOINT and S-Code that promise to improve rail network performance through the use of new mechanisms, monitoring and control systems. This paper focusses on modelling and control of a lab-demonstrator from the REPOINT project. Unlike conventional track switch machines, this actuator needs closed loop feedback control. First, a detailed simulation model of the actuator is developed and validated against experimental results. Two model-based control designs are then developed and tested: a classical cascaded P/PI controller and a modern state feedback controller. The two controllers are compared and it is found that, whilst there are some performance differences, both meet the requirements for use in a redundantly actuated REPOINT switch.**

***Index Terms*—REPOINT switch, PI Control, LQR control, model validation, position control.**

I. Introduction

TRACK switches allow for flexibility on railway networks by enabling railway vehicles to change between routes. Despite their necessity, they are prone to failure and these switch failures can rapidly degrade railway network operations. Unlike road transportation where vehicles can steer around failed vehicles or roadway, in railway systems, vehicles are reliant upon switches in order to change routes. In the event of switch failure, all vehicles attempting to pass through the switch are unable to do so until repair is complete. Track switches are therefore a single point of failure on the railway network with current practice to rectify and prevent failures being maintenance.

A new generation of track switching concepts are emerging from projects such as S-code [1], In2Rail [2] and REPOINT [3]–[4]. improving rail network performance. The proposed REPOINT switch, layout shown in Fig. 1 introduces redundancy in actuation to railway track switching, as exists in safety critical systems, like aerospace flight control and nuclear power plant thermal management. It also has a new mechanical design that incorporates a lift-and-drop switching mechanism replacing the sliding motion that exists today. This design presents benefits in switch reliability, ease of maintenance and increased rail capacity detailed in [3]. In Fig. 1, the three possible routes are shown together with the redundant actuators that are each capable of moving the switch. The main difference between the REPOINT switch and other existing track switches is the use of redundancy in actuation that enables continued rail network operation in the presence of actuator failures alongside a new mechanical design that allows for more than two routes for locomotives through the use of passive locking.

In order to operate a REPOINT switch safely, advanced controller action for each actuator is required to enable coordination of multiple actuators in bending the track while preventing overshoot beyond any of three switch positions. Rail track flexure in the vertical direction for switching operation has not been done before on a railway track. This paper addresses this through the application of different closed loop position feedback controllers to a single REPOINT switch actuator. A detailed mathematical model is developed of the REPOINT concept for controller design. This work in this paper is different from [5] as the work herein includes the detailed process used to define the system parameters in addition to the experimental validation of the model against a laboratory demonstrator.

The model is then linearised to allow for its use as a design model. An investigation of two model-based control strategies from development through to testing of their performance against experimental results is performed. This research work is different from earlier research on the REPOINT concept as this is the first application and validation of model-based closed loop feedback control on the REPOINT laboratory demonstrator. The novel contribution is therefore in the use of closed loop feedback control in order to operate a lift-and-drop railway track switch actuator.

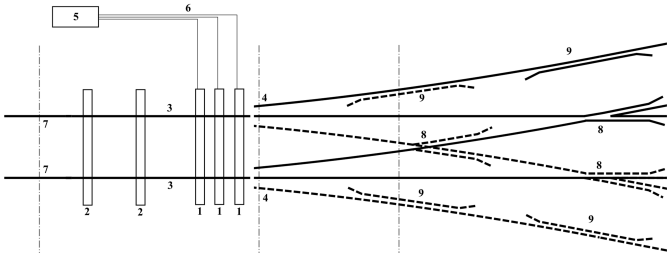

Fig. 1. REPOINT switch layout - 1 *Bearer with electro-mechanical actuator featuring integral passive locking elements*; 2 *Bearer with passive locking elements*; 3 *Stock rails*; 4 *Stub-switch rail ends*; 5 *Control unit*; 6 *Wired connections*; 7 *Straight Route*; 8 *Common crossing*; 9 *Check rails*. [6]

P. L. Kaijuka, C. P. Ward and S. Bemment work in the Control Systems Research group in the Wolfson School of Mechanical, Electrical and Manufacturing Engineering, Loughborough University, LE113TU.
R. Dixon and S.Dutta work in the School of Engineering at Birmingham University
*Corresponding author e-mail: p.l.kaijuka@lboro.ac.uk.
Manuscript received December 3, 2018; revised June 18, 2019.

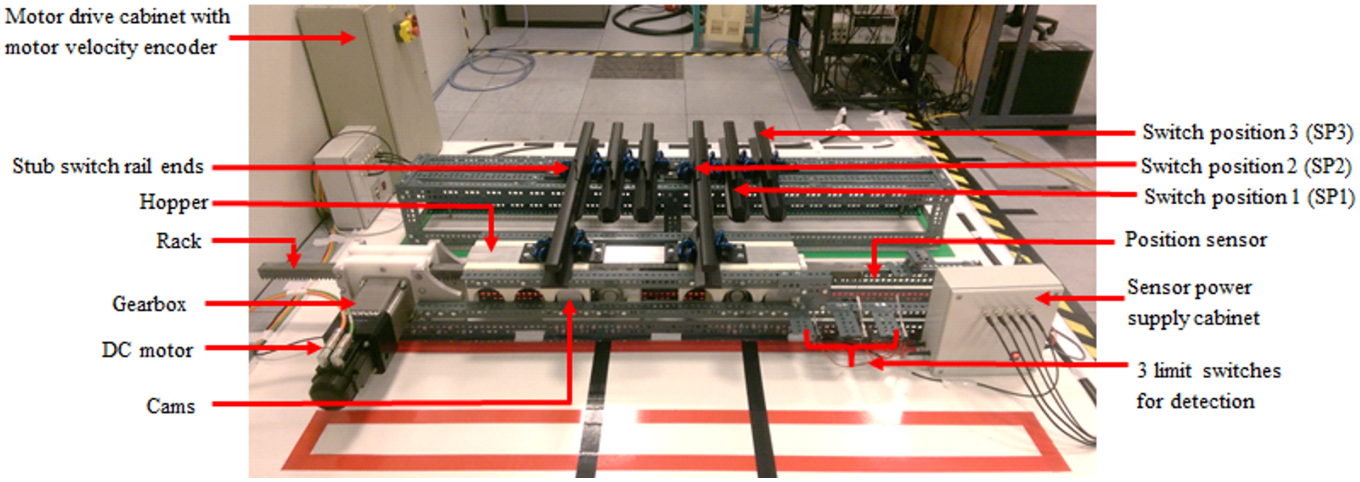

Fig. 2. REPOINT laboratory demonstrator

II. Experimental Setup

The REPOINT laboratory demonstrator, Fig. 2, represents an actuator-bearer for a switch with three routes out. The laboratory demonstrator is sized for the Romney, Hythe and Dymchurch (RHDR) railway track in Kent, United Kingdom [7]. It consists of a three-phase brushless DC motor coupled to a speed reducing gearbox. The gearbox is connected to a rack and pinion drive where the rotary movement of the gearbox provides the linear backward and forward motion in the rack. The rack is connected to two cams and the hopper element via the cam pinions that are driven by the rack. The cams convert the linear motion of the rack into the rotational motion to move the hopper. The hopper element which mounts the switch rail ends is lifted by the cams and moves them through $180°$. Hence, by rotating the motor, the cams are driven and have the effect of lifting (unlocking) the rails and moving them from one switch position to another. The rails shown in Fig.2 are not continuous rails as would be present in a physical track switch. The equivalent rail forces have been replicated by attaching representative spring loads between the hopper and the base attached to the ground.

There are three sensors used in the feedback control of the experimental system. A potentiometer is connected to the end of the rack to measure the position. This measurement corresponds to the track switch positions: leftmost at -0.094 m, centre at 0m and rightmost at 0.094 m as shown in Fig. 2. The motor velocity is measured with an encoder embedded in the motor drive and a current measurement is also provided as an analogue output from the motor drive.

Limit switches are also installed on the demonstrator in order to safeguard the system from running beyond its safe operating range and to replicate current switch methodology where they could be integrated into existing signalling systems if required. MATLAB/Simulink [8] software is used for modelling and simulation together with dSPACE 1104 Control board [9] for the implementation of real-time control on the experimental system.

III. System Modelling

Two types of models are required as part of the control design, commissioning and testing process.

- *Simulation models (often non-linear)*: With dynamics as close as possible to the physical system used to test the designed controller before commissioning on the real system.
- *Design models (usually linear)*: This is a simplification of the model around small operating regions, but still representative of the dynamics of the system used to allow design of the control system

Initial tests of the designed controller on the simulation model allows the designer to gain confidence that the controller will not cause dangerous behaviour of the system when it is applied and tested on the real system itself.

First, in section A, a non-linear simulation model of the REPOINT actuator is developed and described. This simulation model is validated against experimental data obtained from the lab demonstrator in Section B. Finally, in Section C, the simulation model is linearised, simplified and formulated in state-space form as a reduced order design model model which can be used to design the controllers.

A. Nonlinear Simulation Model

The simulation model below describes the physical sub components of the laboratory demonstrator where a MATLAB/Simulink model is shown in Fig. 4.

1) DC Motor and Gearbox: The motor input voltage, V_a drives the motor leading to rotational motion of the motor shaft at a motor speed of $\dot{\theta_m}$. The mathematical equations describing the electrical components of the DC motor shown in Fig. 3 is:

$$V_a = R_a i_a + L_a \dot{i_a} + K_m \dot{\theta_m} \tag{1}$$

where i_a is the motor armature current, R_a is the rotor resistance, L_a is the rotor inductance and K_m is the motor torque constant.

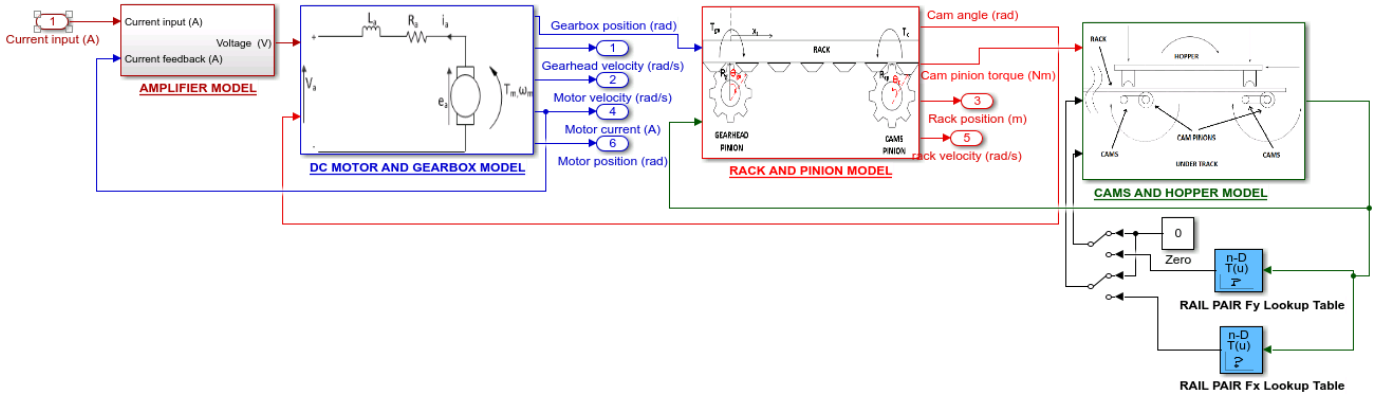

Fig. 4. Simulink simulation model of experimental set up

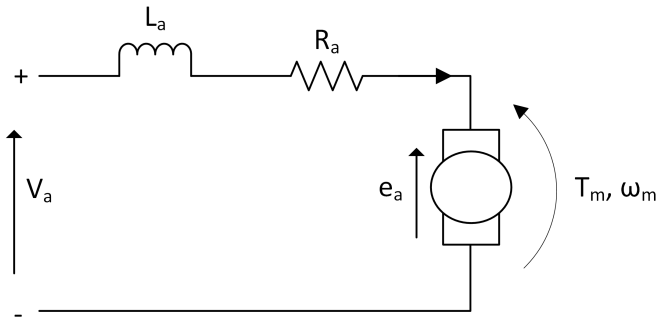

Fig. 3. Electrical schematic diagram of DC motor

Making the assumption that the motor and gearbox are rigidly coupled, the mechanical output torque equation describing the motor torque, is T_m which is proportional to the motor armature current, i_a by a motor torque constant, K_t where $T_m = K_t I_a$.
The gearbox torque, T_g are derived using Newton's second law of motion as:

$$T_m - \frac{T_g}{n} = (J_m + J_g)\ddot{\theta_m} + (B_m + B_g)\dot{\theta_m} \tag{2}$$

The parameter information shown in Table I for the motor and gearbox equations described above are obtained from the Kollmorgen motor and gearbox datasheet used in the experimental setup [10], [11].

TABLE I
DC MOTOR AND GEARBOX PARAMETER VALUES

	Description	Value	Units
R_a	Rotor resistance	1.97	Ω
L_a	Rotor inductance	7.9×10^{-3}	H
e_a	Back emf constant	0.4899	$Vrms/(rad/s)$
J_m	Rotor inertia	0.00034	kgm^2
B_m	Motor damping constant	3.15×10^{-4}	$Nm/(rad/s)$
K_m	Motor torque constant	0.8	Nm/A
B_g	Gearhead damping constant	0.001	$Nm/(rad/s)$
J_g	Gearhead inertia	2.85×10^{-4}	kgm^2
n	Gearhead reduction ratio	70	
	Amplifier proportional gain	0.0016	V/A
	Amplifier integral gain	1×10^6	$(V/A)/s$

2) Rack and pinion: The output of the gearbox is meshed via a spur gear to a linear toothed rack in order to transform the rotational movement by the gear into linear movement of the rack. The mechanical set up of the rack is downward facing with a drive pinion connection to the motor and gearbox and two output cam pinions modelled here as a single cam as shown in Fig. 5.

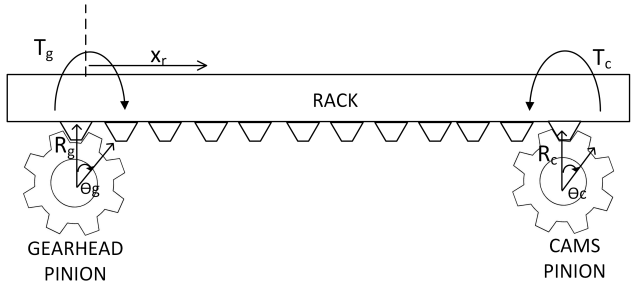

Fig. 5. Schematic diagram of rack and pinion assembly

The mechanical equations of motion describing the movement of the rack and pinion assembly are derived by summing the forces on the rack, where T_c is the cam pinion torque described in the next model section.

$$\frac{T_g}{R_g} - \frac{T_c}{R_c} - b_r\dot{x_r} = m_r\ddot{x_r} \tag{3}$$

The angular position of the rack, θ_r and linear displacement of the rack, x_r are related by:

$$\theta_r = \frac{x_r}{R_g} \tag{4}$$

The equations governing the torque exerted by the gearbox and cam pinions, T_g and T_c respectively on the rack is described as a function of their torsional stiffness, K_g and K_c respectively below and θ_c is the angular position of the cams.

$$T_g = K_g(\theta_g - \theta_r) \tag{5}$$

$$T_c = K_c(\frac{x_r}{R_c} - \theta_c) \tag{6}$$

Some assumptions and approximations have been made in deriving the rack and pinion equations including the following;

- The rack friction coefficient is modelled as a linear term proportional to the rack speed
- The effect of backlash on the rack is ignored as its effect is found to be negligible

The parameter information in Table II for the rack and pinion equations described above are also taken from the manufacturers' datasheets in [12] - [13].

TABLE II
RACK AND PINION PARAMETER VALUES

	Description	Value	Units
R_g	Gearhead pinion radius	0.04	m
R_c	Cam pinion radius	0.03	m
K_g	Gearhead torsional stiffness	1.52×10^5	Nm/rad
K_c	Cam pinion torsional stiffness	1.38×10^5	Nm/rad
m_r	Mass of rack	14.3	kg
b_r	Rack friction coefficient	0.08	N/ms^{-1}

3) Cams and hopper: A cam is a mechanical element used to transmit a rotational motion to a follower by direct contact. The follower is the driven element, in this case the hopper, shown in Fig. 6 on which the rail ends are mounted. The mass of the hopper is balanced across two identical cams.

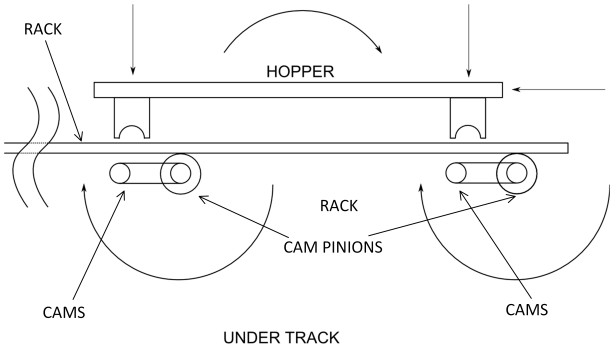

Fig. 6. Cams and hopper movement diagram [5]

The torque governing the movement of the two identical cams is described in the equation below:

$$T_c - R_c(F_x \sin\theta_c + (F_y + mg)\cos\theta_c) = J_c\ddot{\theta}_c + B_c\dot{\theta}_c \quad (7)$$

T_c is the torque applied from the rack to the cam. The forces F_x and F_y due to the full rail pair are included in the simulation model and discussed in the next section. The parameter information for the cam and hopper equations are shown in Table III. These are custom-made parts whose parameters are calculated from basic mechanics and physics formulas [5].

TABLE III
CAM AND HOPPER PARAMETER VALUES

	Description	Value	Units
m	Mass of hopper	20	kg
g	Gravity	9.81	N/kg
R_c	Cam radius	0.08	m
J_c	Cam-hopper inertia	2.28	kgm^2
B_c	Cam-hopper damping coefficient	25	$Nm/Rads^{-}1$

Beyond the basic dynamics Equations [1] - [7], it is also important to include the physical limits of the three outputs present in the experimental system which include; $\pm 9A$ for the motor current, $\pm 450 rad/s$ for the motor velocity and a maximum rack position of $\pm 0.095m$. This is necessary as the controller needs to operate within the maximum physical limits of the system.

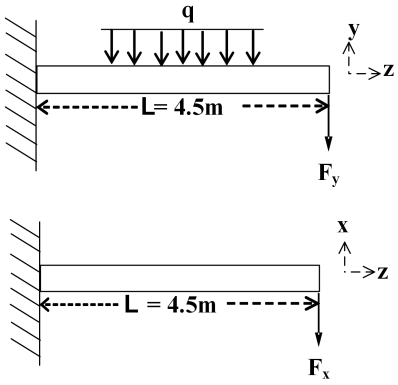

Fig. 7. Rail pair model schematic

4) Rail pair model: As discussed in the cam and hopper model, the vertical and horizontal forces due to the rail pair shown in Fig. 7 are present on a physical railway switch and these parameters are given in Table IV. Lumping the rail pair as a single beam, the beam deflection using McCaulay's method for the deflection of beams [14] and taking moments about the anchor point, the rail pair bending moment M_{y-z} in the vertical direction (y-z axis) is:

$$M_{y-z} = F_y z - \frac{q}{2}z^2 \quad (8)$$

The rail pair magnitude of deflection in the vertical direction, δy and vertical force, F_y is calculated as:

$$EI_{yy}\delta y = F_y\frac{z^3}{6} - \frac{q}{24}z^4 + C_1 z + C_2 \quad (9)$$

where q is an evenly distributed load, $C_1 = \frac{qL^3}{6} - \frac{L^2}{2}F_y$ and $C_2 = \frac{q}{24}z^4 - \frac{q}{6}L^4 + \frac{L^3}{2}F_y - \frac{z^3}{6}F_y$.

Similarly in the horizontal direction, the forces are calculated without an evenly distributed load, q. The bending moment, M_{x-z} in the horizontal direction (x-z axis) is:

$$M_{x-z} = F_x z \quad (10)$$

The rail pair magnitude of deflection in the horizontal direction, δx and vertical force, F_x is calculated as:

$$EI_{xx}\delta x = F_x\frac{z^3}{6} + C_3 z + C_4 \quad (11)$$

where $C_3 = -\frac{L^2}{2}F_x$ and $C_4 = \frac{L^3}{3}F_x$.

TABLE IV
RAIL PAIR PARAMETERS

	Descrption	Value	Units
q	Rail section mass	17.4	kg
Ixx	Area moment of inertia (x-z)	$1.594e-5$	m^4
Iyy	Area moment of inertia (y-z)	$3.36e-5$	m^4
E	Elastic modulus	$200e9$	Pa
L	Length to fixed point from actuator	4.5	m

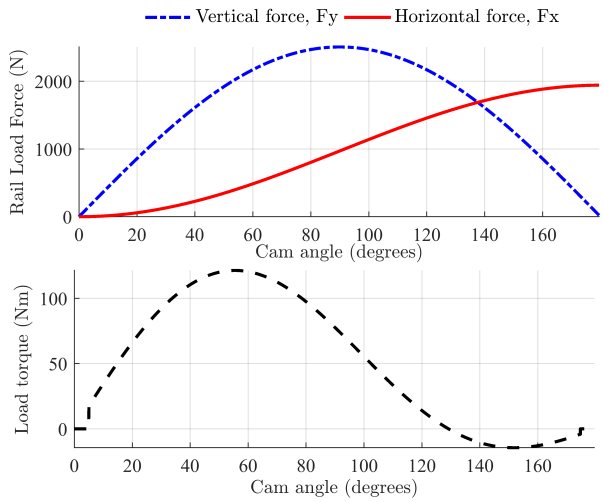

Fig. 8. Rail pair load against cam angle

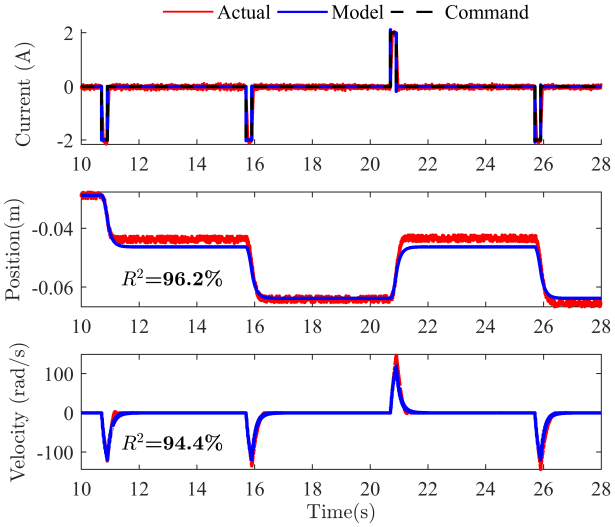

Fig. 9. Model validation against experimental measurements - Test 1

The purpose of modelling the rail pair forces is to provide a horizontal and vertical load that the rail load will apply on the cams. Fig. 8 below shows these forces for a single switch movement rotating through $180\,\text{deg}$.

5) Motor Amplifier model: In practice, as is the case in this system, the motor drive usually contains an embedded current PI controller leaving two control variables: motor velocity and rack position. This inbuilt current PI controller is also included in the simulation model with gains shown in Table I and used for validation purposes as shown in Fig. 4. The PI controller values are provided in the motor drive. The first step in the model validation was in the comparison of the experimental inbuilt current PI controller against the simulated PI controller. These results matched up giving confidence in the use of this PI controller for the rest of the system validation. Identification of the parameters was therefore not required and no issues were identified in the use of the PI controller for the model validation process. A systematic process for experimental validation was then followed as the physical motor and system parameters are available from the manufacturer data sheets.

B. Simulation model validation

Experimental data is used to validate the simulation model. The system is run with the rack position and motor velocity in the open-loop with no feedback control alongside the inbuilt current controller in the motor drive. The same current command input pulse of $2A$ is applied to the simulation model and experimental system. The model is validated against the system yielding results in Fig. 9 and 10. This shows a good match between the model and measured responses with high coefficient of determination (R^2) values for rack position and motor velocity. The minor discrepancies present are due to the non-linearities present in the physical system. Despite this, the model is a good representation of the system and is considered valid. A number of experiments were run to validate the open loop model with varying inputs and these results are omitted for brevity. Overall the simulation results against the experimental results show the model is a good fit.

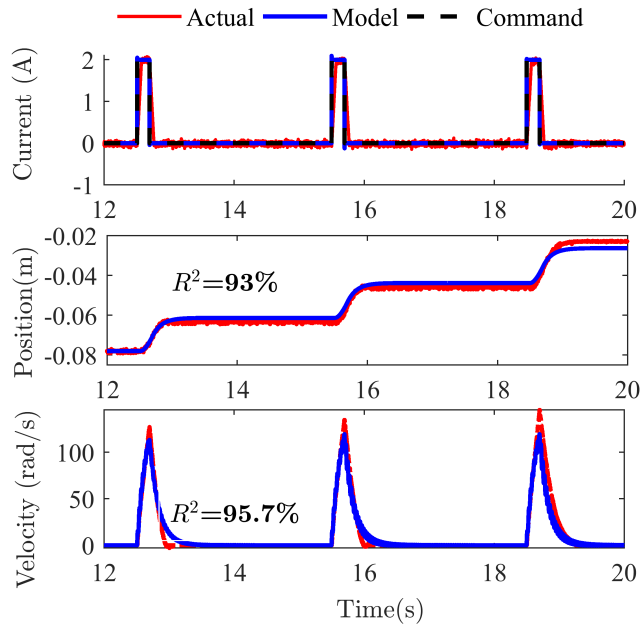

Fig. 10. Model validation against experimental measurements - Test 2

C. Design model

A reduced order linear design model of the system is developed by making some assumptions:

- Rigid interconnections exist between the subsystems by reflecting the equivalent rack and pinion and cams damping to the motor shaft as, D_{sum} and total inertia from the two as, J_{sum} assuming an infinitely stiff motor load
- Removing the non-linear terms including the limit switches and physical maximum limits of the system
- Due to the inbuilt current controller, it is also assumed that the input current demand and the current feedback are equal
- The rail load torque, T_l can be modelled as an external input disturbance

By making these assumptions, it is possible to obtain a 2nd order design model in state-space form.

$$\dot{x} = \mathbf{A}x + \mathbf{B}u \tag{12}$$

$$y = \mathbf{C}x. \tag{13}$$

The state vector, $x(t)$ is therefore converted from an 8th order model derived from Equations (1) - (11) into a 2nd order model constituting two states of the system; motor velocity, $\dot{\theta_m}$ and rack position, x_r:

$$x = \begin{bmatrix} \dot{\theta_m} & x_r \end{bmatrix}^T \tag{14}$$

where the input, $u(t)$ is a motor current input, $i(t)$ with an external rail load torque disturbance input, T_l:

$$u = \begin{bmatrix} i & T_l \end{bmatrix}^T \tag{15}$$

The continuous time state variable equation, **x** for the design model is then described as follows:

$$\mathbf{A} = \begin{bmatrix} -D_{sum}/J_{sum} & 0 \\ Rgp/n & 0 \end{bmatrix} \tag{16}$$

$$\mathbf{B} = \begin{bmatrix} Kt/J_{sum} & 0 \\ 0 & 1/J_{sum} \end{bmatrix} \tag{17}$$

$$\mathbf{C} = \begin{bmatrix} 1 & 0 \\ 0 & 1 \end{bmatrix} \tag{18}$$

IV. Controller Design studies

As this is a track switching system, the role of the controller is to track the switch position. The main aim of the feedback control on the REPOINT switch actuator is to move the switch to the demanded position quickly and accurately.

In normal operation mode of a single REPOINT switch actuator in response to a step input, the control requirements are listed below:

- To track a step position demand to any of the three track positions: 0.094m, 0m and -0.094m
- Settling time $<$ 4 seconds
- Rise time $<$ 2 seconds
- 0% overshoot on position
- 0% steady-state position error
- Gain margin $\geq$ than 6dB
- Phase margin $\geq 60^\circ$

In this section, a classical and modern controller are designed, tested and evaluated by analysing their performance against the laboratory demonstrator.

Three feedback variables are available; motor current, motor speed and rack position. However control is only applied to the motor velocity and rack position as the current control loop is an integral part of the motor drive as seen in the model validation section.

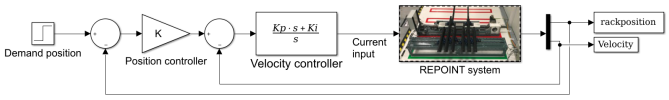

Fig. 11. Simulink model of cascaded P/PI controller design

A. Classical Controller design

A motor positioning system typically consists of a cascaded loop controlling three variables; current, velocity and position. In the present case, the current controller is already included in the amplifier. Hence, the classical controller designed is in the form of a Proportional/Proportional-Integral (P/PI) controller for rack position and motor velocity as shown in Fig. 11. The control input law in the PI controller is defined as:

$$u = K_p e + K_i \int_{t_o}^{t} e dt \tag{19}$$

and the controller gains are determined using classical frequency methods where K_p is the proportional gain and τ_i is the integration time constant. K_i is the integral gain that is equivalent to $\frac{K_p}{\tau_i}$. The outer loop input is the error signal, e_{pos} generated from:

$$e_{pos} = x_d - x \tag{20}$$

where x_d is the desired track switch position and the measured rack positon, x. The inner loop gain input is the error signal, e_{vel} generated from the velocity demand, $\dot{\theta_{md}}$ and velocity feedback, $\dot{\theta_m}$.

$$e_{vel} = \dot{\theta_{md}} - \dot{\theta_m} \tag{21}$$

The P/PI controller gain therefore has three gains: The proportional gain, K that controls the rack position and the proportional gain, K_p and integral gain, K_i that control motor velocity. The output of the PI gain generates the current control input, $u(t)$. The P/PI controller gains are tuned using classical methods by evaluating the gain and phase margins on a Nichols plot.

TABLE V
P/PI Controller values

	Velocity control	Positon control
Proportional gain	0.02 A/ms^{-1}	2300 s^{-1}
Integral time constant	0.06 s	

The achieved stability margins are shown in the Nichols plot in Fig. 12 derived using the control gains described. The Nichols plot shows the rack position output response for the designed controller. The phase margin of 88.1° and gain margin of $110db$ dB are greater than the minimum control requirements of 60 °and 6dB, respectively.

1) Application and test of Classical Controller: The classical controller designed above with control gain values in Table V is first tested on the simulation model before application on the experimental system. In both cases a step input from SP1 to SP2 (0m to 0.094m) is applied as the controllers are required to track the switch position hence the use of a reference tracking

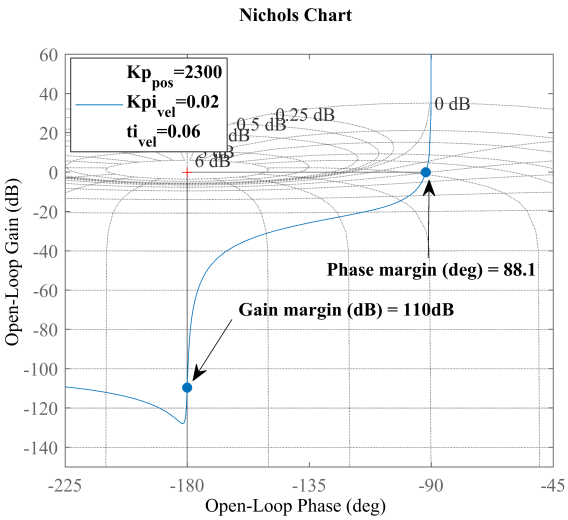

Fig. 12. Nichols plot for P/PI controller

test. The results can be seen in Fig. 13 which show the rack positions and velocity responses respectively.

It can be seen that the simulated response and real response are similar with differences due to noise and other unmodelled effects. This confirms the merit of using the simulation model to predict the performance before applying to the real system (which can transmit large forces and rapid accelerations if it goes unstable).

It is also clear that the resulting closed-loop system meets the step response requirements; with a rise time of 1.55 seconds, zero overshoot and no steady state error.

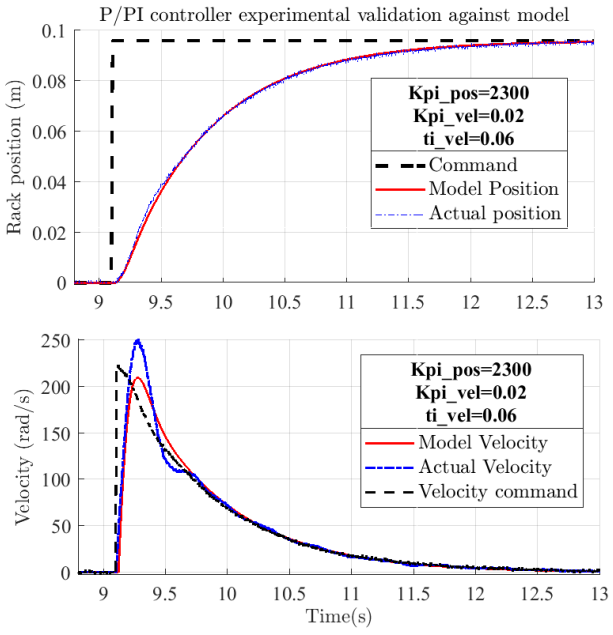

Fig. 13. P/PI controller step response experimental validation

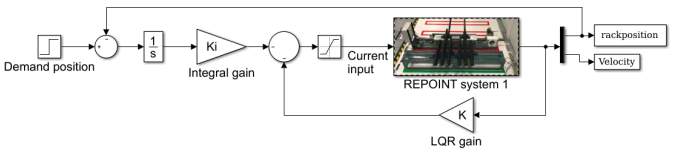

Fig. 14. REPOINT system with LQI control

B. Linear Quadratic Regulator with Integral Action (LQI) Controller Design

The Linear Quadratic Regulator (LQR) controller is an optimal control technique that provides a systematic way of calculating the state feedback gains. The LQR controller assumes the system to be linear for its design and the system must be controllable [15], which the design model in Equations (12) - (18) satisfies. For this controller design, the states of the system are measurable and therefore there is no need for observer design. The design model meets the controllability requirement and is used to design the LQR controller.

The LQR state feedback control law where the current input, u, system states, x: motor velocity, $\dot{\theta_m}$ and rack position, x_r and LQR controller gain matrix, K are defined as:

$$u = -Kx \tag{22}$$

To maintain the desired output position, integral action is included in the LQR controller design to form a Linear Quadratic Integral (LQI) controller. The Integral gain, K_i removes the steady-state error of the output track switch position. The state space equation describing the system is augmented to the state space equation in (23) below in order to introduce integral action [15].

$$\begin{bmatrix} \dot{x} \\ \dot{e} \end{bmatrix} = \begin{bmatrix} A & 0 \\ -C & 0 \end{bmatrix} \begin{bmatrix} x \\ e \end{bmatrix} + \begin{bmatrix} B \\ 0 \end{bmatrix} u + \begin{bmatrix} 0 \\ I \end{bmatrix} r \tag{23}$$

C is the output matrix, e is the integral of position error and r is the reference input.

The state feedback law of Equation 22 is modified as shown in Fig. 14 to Equation 24.

$$u = \begin{bmatrix} K & -Ki \end{bmatrix} \begin{bmatrix} x \\ e \end{bmatrix} \tag{24}$$

Given the state space system described in the design model section of this paper, the LQR gain, K is chosen such that it minimises the quadratic cost function, J, below:

$$J = \int_0^{\inf} (x^T Q x + u^T R u) dt \tag{25}$$

where Q is a 2×2 weighting matrix and R is a scalar chosen to provide a trade off between penalising the states and the control efforts of the system respectively [16]. This is obtained by solving the algebraic Ricatti equation below:

$$A^T S + SA - SBR^{-1}B^T S + Q = 0 \tag{26}$$

where

$$K = R^{-1}B^T S. \tag{27}$$

In order to tune the LQI control gains, the initial step taken was to follow Bryson's rule [17] that suggests the Q and R matrices are chosen such that:

$$Q_{ii} = \frac{1}{\text{maximum acceptable value of } {x_i}^2} \tag{28}$$

$$R = \frac{1}{\text{maximum acceptable value of } u^2} \tag{29}$$

The Q and R values are then further modified to better match the desired transient response of the system and to meet the stability requirements as shown in Fig. 15. The chosen weightings on the input current and states, R and Q respectively and derived control gains, K and K_i in MATLAB are shown in Table VI.

TABLE VI
LQI CONTROLLER GAINS

R	0.1
Q	diag[$8.1/0.09^2$ $2/200^2$ $50/0.1^2$]
K	[185 0.0179]
K_i	-223.6

The stability margins for the LQI controller meet the control requirements as shown in the Nichols plot with the chosen gains achieving a gain margin of inf and phase margin of 86.7°.

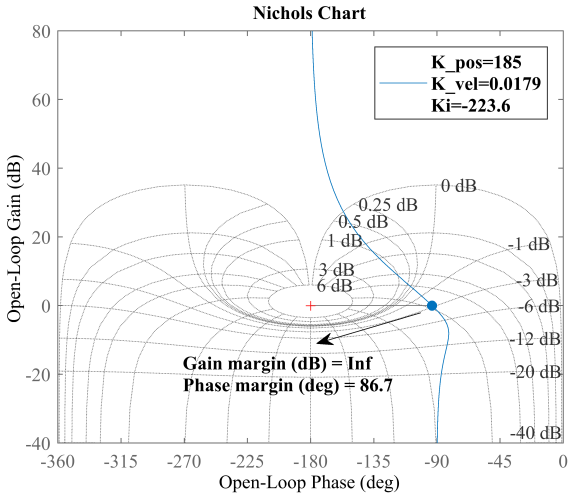

Fig. 15. Nichols plot for designed LQI controller

1) Experimental Validation - LQI Controller: The designed LQI controller is applied to the REPOINT laboratory demonstrator. Similar to the PI controller, a step position input demand from SP1 to SP2 of 0.094m is applied to the real system using the LQI controller gain values in Table VI and the system and model response compared as shown in Fig. 16.

As position control, is the main objective of the controller, it is evident in Fig. 16 that the requirements of rise time, overshoot and steady state error are satisfied. The model also closely matches the actual position measurements from the system.

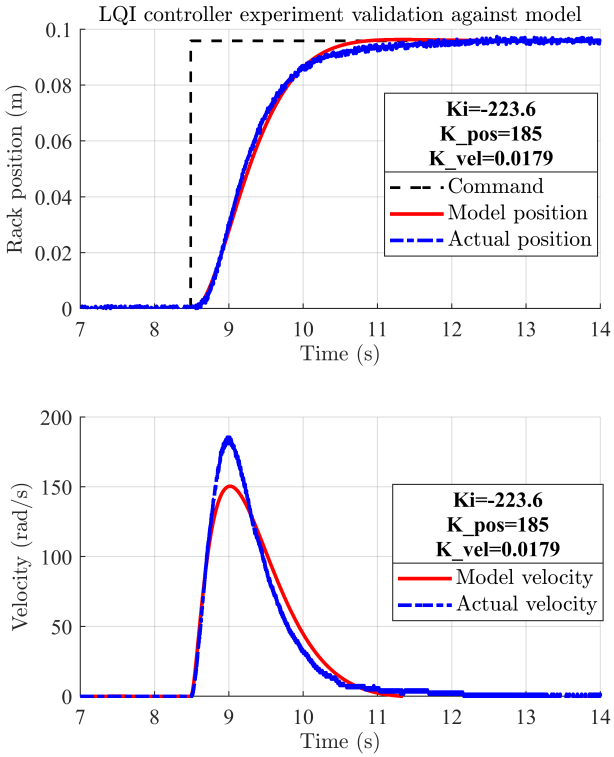

Fig. 16. LQI controller step response experimental validation

C. Comparison of Control methods

In order to compare the two controllers, the designed P/PI and LQI controllers are applied on the system and their performance evaluated as shown in Fig. 17. As shown in Table VII, the LQI controller displays slightly better performance by reaching steady state faster and drawing less current. The P/PI controller gains could be increased to achieve faster switching time however this would lead to greater current input required to operate the switch requiring increased power demand which is undesirable for this application.

TABLE VII
COMPARISON OF CONTROLLER PERFORMANCE

	LQI	P/PI
Rise time	1.19 s	1.55 s
Settling time	2.36 s	2.66 s
Overshoot (%)	0	0
Peak Velocity	184 rad/s A	250 rad/s
Control input peak	2.1 A	2.7 A

Another track switching scenario using both controllers is tested where the track switch is moved continuously between the three track switch positions: 0 m (SP1), 0.094 m (SP2) and -0.094 m (SP3) and the controller performance evaluated. The results shown in Fig. 18 also show the controllers satisfy the performance requirement when used to move the switch between varying positions. It is also further evident that the LQI controller draws less current to move the switch to the required position at a slightly faster rise time than the P/PI

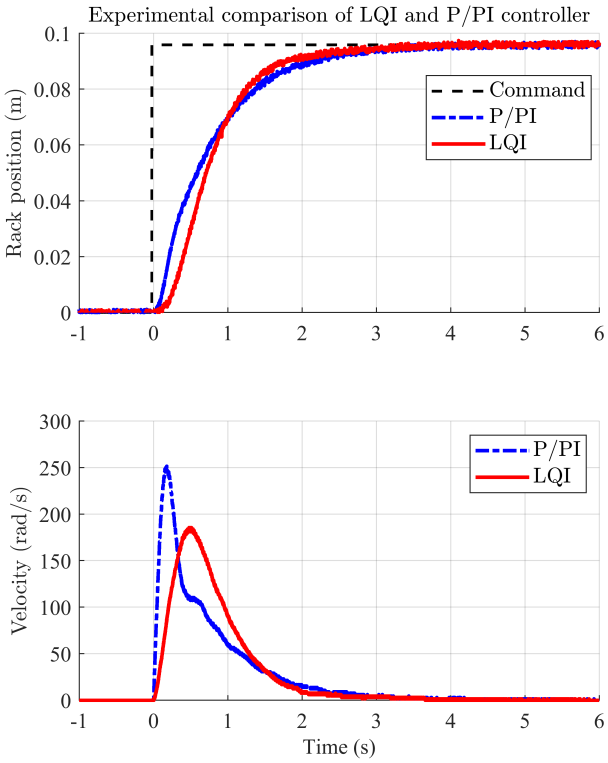

Fig. 17. Experimental comparison of P/PI and LQI controller

controller. These results are a select illustrative number of experiments that were part of a larger controller validation process. These are omitted for brevity.

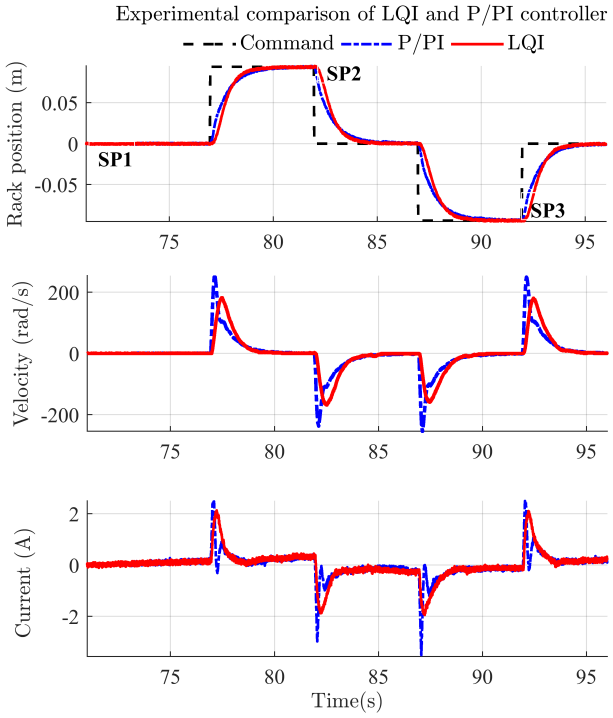

Fig. 18. Experimental comparison of controller design

During experimental tests, it was noted that there are not many disturbances to the system. The main disturbance is sensor noise on the system which the controller tolerates. Other non-linearities in the real system included; backlash in the gears and current deadzone which were overcome by the controller. The controller is also robust to parameter changes where the most significant change in the real application would be the variation in the rail load depending on the number of actuators moving the rail. In order to demonstrate the controllers ability to cope with this, external spring loads representing the peak rail forces when a single actuator is used as calculated in Fig. 8 are added to the system pictured in Fig. 19. The LQI controller is applied for this test and it is seen that the the controller is robust to these changes and the control requirements to follow a step change in position are met as in Fig. 20 with more current draw to the system in order to overcome the load.

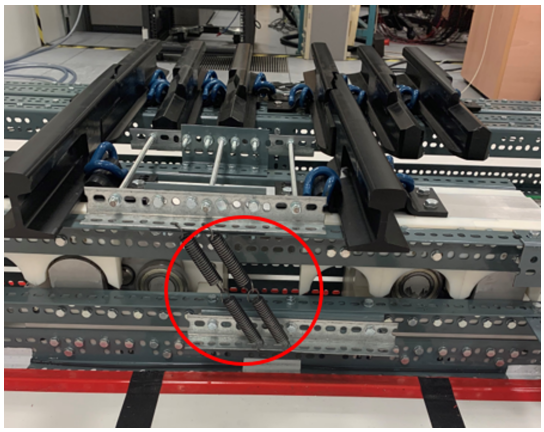

Fig. 19. REPOINT actuator with equivalent rail load

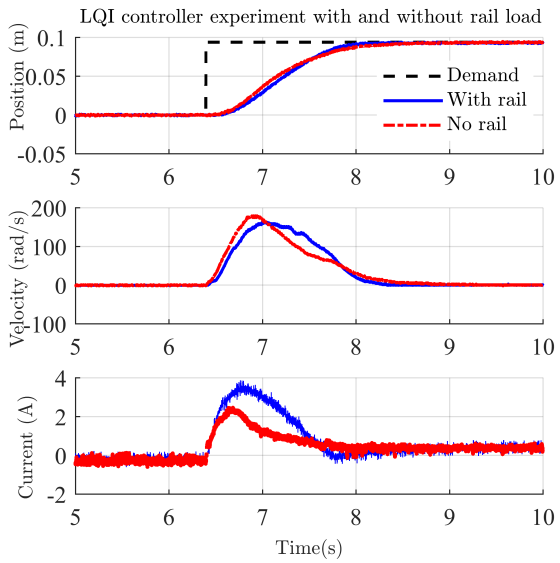

Fig. 20. LQR control with and without rail load

Further comparison of the rail bending peak static forces for a Network Rail traditional CVS switch size [18] against the RHDR rail scale switch peak forces analysed in Fig. 8

is performed. It is seen that the peak forces and the scales of the system are proportional and therefore the hypothesis is that these controllers will also tolerate the non-linear dynamics present in a full-size Network Rail switch.

V. Conclusion

This paper has focussed on modelling and control design for the REPOINT laboratory demonstrator. A non-linear simulation model has been developed based on the physics of the system. It has then been validated against experimental measurements from the real system, where it is found that the mathematical model provides a good representation of the dominant dynamics of the system. A simplified linear model has then been extracted, which is used for controller design. The design of two controllers has been carried out and they have both been tested on the full simulation model, and then implemented and tested on the real system.

The implementation tests also showed that both the classical control and modern controller could achieve effective position control which met the specified control requirements for the system. It is observed that the non-linearities in the real system including sensor noise, backlash in the rack and pinion and gears in addition to current dead zone were tolerated by the controller.

Overall, the modern controller showed slightly better performance requiring a lower peak control input to attain a faster rise time and settling time. The classical controller however draws more current input than the modern controller to achieve a similar switching time. The modern controller is therefore preferred as it meets the control requirements and requires less current input to achieve track switch position within the physical limits of the system.

The excellent performance of both controllers on the lab demonstrator of the REPOINT switch actuator, suggests that such a closed-loop actuation system might be successfully used for control of a real switch. Future work will include validating this controller for use in a complete REPOINT switch with three actuator-bearers, in order to demonstrate redundancy of actuation. The overall intention is that through introduction of redundancy in railway track switching, rail network performance could be drastically improved in the areas of availability and reliability.

Acknowledgment

The authors would like to thank Loughborough University and Railway Safety and Standards Board (RSSB) for funding this PhD study.

References

[1] "S-Code." [Online]. Available: http://www.s-code.info/
[2] "In2Rail." [Online]. Available: http://www.in2rail.eu/
[3] S. D. Bemment, R. M. Goodall, R. Dixon, and C. P. Ward, "Improving the reliability and availability of railway track switching by analysing historical failure data and introducing functionally redundant subsystems," *Proceedings of the Institution of Mechanical Engineers, Part F: Journal of Rail and Rapid Transit*, sep 2017.
[4] P. Kaijuka, R. Dixon, and C. Ward, "Active fault tolerant control applied to REPOINT, a novel railway track switch," *IFAC-PapersOnLine*, vol. 51, no. 24, pp. 529–535, jan 2018.
[5] N. Wright, S. Bemment, C. Ward, and R. Dixon, "A model of a repoint track switch for control," *2014 UKACC International Conference on Control, CONTROL 2014 - Proceedings*, pp. 549–554, 2014.
[6] T. Harrison, S. D. Bemment, E. Ebinger, R. M. Goodall, C. P. Ward, and R. Dixon, "Rethinking Rail Track Switches for Fault Tolerance and Enhanced Performance," *IFAC-PapersOnLine*, vol. 49, no. 21, pp. 260–266, jan 2016.
[7] Rhdr.org.uk, "Romney, Hythe & Dymchurch railway." [Online]. Available: http://www.rhdr.org.uk/
[8] MathWorks, "MATLAB Documentation - MathWorks United Kingdom." [Online]. Available: https://uk.mathworks.com/help/matlab/
[9] DSPACE, "DS1104 R&D Controller Board - dSPACE." [Online]. Available: https://www.dspace.com/en/pub/home/products/hw/singbord/ds1104.cfm
[10] Kollmorgen, "AC Synchronous Servo Motors — Kollmorgen." [Online]. Available: http://www.kollmorgen.com/en-us/products/motors/servo/akm-series/akm-series-ac-synchronous-motors/ac-synchronous-servo-motors/
[11] TRUE Planetary Gearheads - Kollmorgen, "TRUE Planetary Gearheads." [Online]. Available: https://www.kollmorgen.com/sites/default/files/public{_}downloads/True{_}Planetary{_}Gearheads{_}Installation{_}en-US{_}rev2008.pdf
[12] HPC Gears - Spur Gear, "YG4. Spur Gear. HPC." [Online]. Available: http://www.hpcgears.com/pdf{_}c33/23.68-23.73.pdf
[13] HPC Gears - Steel Spur Rack, "CR. Steel Spur Rack. HPC." [Online]. Available: http://www.hpcgears.com/pdf{_}c33/22.3.pdf
[14] W. H. Macaulay, "Note on the deflection of the beams," *Messenger of Mathematics*, 1919.
[15] B. D. O. Anderson and J. B. Moore, *Optimal control : linear quadratic methods*. Prentice Hall, 1990.
[16] K. Ogata, *Modern control engineering*. Prentice-Hall, 2010.
[17] G. F. Franklin, J. D. Powell, and A. Emami-Naeini, *Feedback control of dynamic systems*. Pearson, 2015.
[18] M. Sarmiento-Carnevali, T. J. Harrison, S. Dutta, S. D. Bemment, C. P. Ward, and R. Dixon, "Design, construction, deployment and testing of a full-scale Repoint Light track switch (I)," *Stephenson Conference: Research for Railways*, 2017. [Online]. Available: https://dspace.lboro.ac.uk/dspace-jspui/handle/2134/25853

Precious Kaijuka received an MEng degree in Electrical and Electronic Engineering from Loughborough University in 2013. She is currently working towards her PhD degree in the Wolfson School of Mechanical, Electrical and Manufacturing Engineering at Loughborough University. Her research interests include system modelling, control design and fault tolerant control of mechatronic systems. She is a Member of the Institution of Engineering and Technology (MIET)

Roger Dixon is a Professor of Control Systems Engineering in Birmingham University School of Engineering. His research focuses on various aspects of control systems engineering including: application of model-based control systems design, model-based fault detection and isolation, system condition/health monitoring and fault tolerant design of controllers and actuators.

Christopher Ward is a Senior Lecturer in the Wolfson School of Mechanical, Electrical and Manufacturing Engineering and is the Head of the Control Systems Group. His current research work is concentrated on control and fault detection in railway vehicle based problems, particularly focusing on the critical wheel/rail contact area. Chris has a PhD in Automotive Engineering and BEng in Mechanical Engineering. He is a Chartered Engineer and a Member of the Institution of Mechanical Engineers.

Saikat Dutta is a Research Associate at Birmingham University, UK. His current research work is focused on innovative railway track switching systems. He has previously worked as a post-doctoral fellow in Smart Structures and Systems Laboratory, in Inha University, South Korea. He received his PhD from Indian Institute of Technology Kharagpur, India in Mechanical Engineering researching vibration isolation using Magneto-rheological dampers.

Samuel Bemment received the Bachelor's degree in Aeronautical Engineering from Loughborough University, UK, in 2009. He worked for the UK rail infrastructure custodian, Network Rail before returning to Loughborough to as an R&D engineer on the REPOINT project. He completed his PhD at Loughborough University in 2018 and his research interests include rail signalling, practical applications of condition monitoring and fault detection, and rail performance metrics.